AGU ADVANCING EARTH AND SPACE SCIENCES

JGR Space Physics

RESEARCH ARTICLE
10.1029/2023JA032290

Statistical Properties of Quasi-Periodic Electromagnetic Ion Cyclotron Waves: ULF Modulation Effects

Muhammad Shahid[1,2], M. Fraz Bashir[2], A. V. Artemyev[2,3], X.-J. Zhang[2,4], Vassilis Angelopoulos[2], and G. Murtaza[1]

[1]Salam Chair in Physics, Government College University Lahore, Lahore, Pakistan, [2]Department of Earth, Planetary, and Space Sciences, University of California, Los Angeles, CA, USA, [3]Space Research Institute, Russian Academy of Sciences, Moscow, Russia, [4]Department of Physics, University of Texas at Dallas, Richardson, TX, USA

Abstract Electromagnetic ion cyclotron (EMIC) waves effectively scatter relativistic electrons in Earth's radiation belts and energetic ions in the ring current. Empirical models parameterizing the EMIC wave characteristics are important elements of inner magnetosphere simulations. Two main EMIC wave populations included in such simulations are the population generated by plasma sheet injections and another population generated by magnetospheric compression due to the solar wind. In this study, we investigate a third class of EMIC waves, generated by hot plasma sheet ions modulated by compressional ultra-low frequency (ULF) waves. Such ULF-modulated EMIC waves are mostly observed on the dayside, between magnetopause and the outer radiation belt edge. We show that ULF-modulated EMIC waves are weakly oblique (with a wave normal angle $\approx 20^\circ \pm 10^\circ$) and narrow-banded (with a spectral width of $\sim 1/3$ of the mean frequency). We construct an empirical model of the EMIC wave characteristics as a function of *L*-shell and MLT. The low ratio of electron plasma frequency to electron gyrofrequency $\left(f_{pe}/f_{ce} \sim 5 - 10\right)$ around the EMIC wave generation region does not allow these waves to scatter energetic electrons. However, these waves provide very effective (comparable to strong diffusion) quasi-periodic precipitation of plasma sheet protons.

Key Points:

- We conduct statistics of quasi-periodic EMIC waves modulated by compressional ultra-low frequency (ULF) waves
- Most ULF-modulated EMIC waves are observed on dayside magnetosphere at $L \in [8, 12]$
- We construct an empirical model for EMIC wave characteristics as a function of *L*-shell and *MLT*

Supporting Information:

Supporting Information may be found in the online version of this article.

Correspondence to:

M. F. Bashir,
frazbashir@epss.ucla.edu

Citation:

Shahid, M., Bashir, M. F., Artemyev, A. V., Zhang, X.-J., Angelopoulos, V., & Murtaza, G. (2024). Statistical properties of quasi-periodic electromagnetic ion cyclotron waves: ULF modulation effects. *Journal of Geophysical Research: Space Physics*, *129*, e2023JA032290. https://doi.org/10.1029/2023JA032290

Received 17 NOV 2023
Accepted 23 OCT 2024

1. Introduction

Electromagnetic ion cyclotron (EMIC) waves are the primary wave mode responsible for scattering and heating of cold ions (e.g., Kitamura et al., 2018; Ma et al., 2019; Yuan et al., 2016) and precipitating relativistic electrons in the inner magnetosphere (see, e.g., Angelopoulos et al., 2023; Bashir et al., 2022a; Drozdov et al., 2022; Millan & Thorne, 2007; Usanova et al., 2014; Yahnin et al., 2017, and references therein). These waves can be generated by hot, transversely anisotropic ions injected from the plasma sheet and drifting duskward (e.g., Bashir et al., 2022a; L. Chen et al., 2010; Jun et al., 2019, and references therein). This localized region of EMIC generation leads to the prevalence of EMIC wave driven relativistic electron precipitation at the nightside/dusk flank (see Thorne et al., 2006). These relativistic electron losses are well studied theoretically (see reviews by Lee et al., 2021; Thorne et al., 2006, and references therein) and observationally (e.g., Blum et al., 2015; Capannolo et al., 2019, 2023; Yahnin et al., 2016). At dayside, EMIC wave generation is associated with ion anisotropic heating by solar wind compression of the magnetosphere (N. Liu et al., 2022; Xue et al., 2023). The extreme examples of such solar wind driven EMIC wave generation are magnetosphere impact by interplanetary shock waves (Blum et al., 2021; Li et al., 2022; Yan et al., 2023) and solar wind pressure pulses (Xue et al., 2022). Alternatively, EMIC waves can also be generated by another mechanism on the dayside. This mechanism involves intense, compressional ultra-low frequency (ULF) waves that may magnetically trap anisotropic, hot-ion populations and transport them into the inner magnetosphere. Such ULF waves are often generated in response to the magnetopause impact by solar wind/magnetosheath transients (e.g., M. D. Hartinger et al., 2013, 2014; Wang et al., 2018; Wang, Nishimura, et al., 2019). Another ULF mode capable of hot ion trapping and transport is the drift mirror mode (e.g., Hasegawa, 1969): nonlinear mirror mode waves are local magnetic field depletions filled with transversely anisotropic hot ions (Balikhin et al., 2009; Cooper et al., 2021; Rae et al., 2007; Soto-Chavez et al., 2019). Nonlinear mirror waves are generated around the magnetopause and can transport the trapped ion population earthward (due to the convection electric field), where a higher cold background density changes the stability conditions of this population and may drive EMIC wave generation within mirror modes (Kitamura et al., 2021; Loto'Aniu et al., 2009; S. Liu et al., 2019; Z. Y. Liu et al., 2022; Yin et al., 2022). In contrast to EMIC waves generated by plasma sheet ion injections (e.g., Jun et al., 2019, 2021) and thus parameterized by geomagnetic indexes and solar wind conditions (e.g., H. Chen, Gao, Lu, & Wang, 2019; Gamayunov et al., 2020;

Ma et al., 2015; Ross et al., 2021; Usanova et al., 2012), the ULF-associated EMIC waves are not expected to strongly correlate with geomagnetic conditions; instead, they should be mostly determined by dayside magnetosphere interaction with mesoscale (or even ion kinetic scale) transients. Thus, this EMIC wave population may be smoothed out in an index-based empirical model and requires alternative parameterization for further incorporation into simulations of the radiation belt dynamics in the inner magnetosphere. Such ULF-associated EMIC waves may play an important role in relativistic electron precipitation at higher L-shells, well outside the plasmapause (see statistics of relativistic electron precipitation events at high-L in Capannolo et al., 2022). Moreover, the small scale of mirror mode structures (the primary source of ULF-modulated EMIC waves (Bashir et al., 2022b; Shahid et al., 2024)), relative to the typically large-scale EMIC wave generation region (Blum et al., 2016, 2017) may explain the temporally and spatially localized EMIC-driven electron precipitation in observations (Shumko et al., 2022). Additionally, EMIC waves are also responsible for the scattering and isotropization/precipitation of ring current ions (e.g., Jordanova et al., 2001, 2007; Khazanov et al., 2007). Therefore, EMIC wave modulation/generation within mirror-mode structures indicates the solar wind impacts on ring current dynamics.

This study aims to investigate the characteristics of ULF-modulated EMIC waves statistically, their spatial distribution (in L-shell, MLT), and the associated plasma conditions. We analyze 5 years (2017–2021) of THEMIS E, (Angelopoulos, 2008) measurements in the inner magnetosphere and near-Earth plasma sheet. The collected data set contains 330 intervals (each interval represents a period with observations of multiple EMIC bursts associated with ULF waves; the beginning/end of intervals are determined by spacecraft entrance/exit into/from the region of EMIC wave correlation with ULF waves) with multiple EMIC wave bursts modulated by compressional ULF waves, with a total of 1,555 individual bursts (each of them is within the $\sim 1/2$ period of the simultaneously observed ULF wave). Section 2 describes typical events from our data set, whereas Section 3 provides statistical properties of EMIC waves and surrounding plasma characteristics. The development of the empirical model is discussed in Section 4 and the estimation of pitch angle scattering based on the empirical model is provided in Section 5. The results are discussed and concluded in Section 6.

2. Spacecraft Instruments and Data Set

We examine data from three inner probes of the THEMIS mission at an apogee of ∼12 Earth radii (R_E). These probes are equipped with identical instruments (Angelopoulos, 2008). For investigation of EMIC waves, we use: Fast Survey (1/4s sampling) measurements of the fluxgate magnetometer (FGM, see Auster et al., 2008), spin averaged (3s) measurements of ion and electron <30 keV spectra and moments by the electrostatic analyzer (ESA, see McFadden et al., 2008), cold plasma density derived from the spacecraft potential (Bonnell et al., 2008). Details of the method of plasma density evaluation from the spacecraft potential can be found in (Pedersen et al., 1998), whereas estimates of uncertainties of this method in application to THEMIS data set are provided in (Nishimura et al., 2013). Following this uncertainty estimation procedure, we compare the density from the spacecraft potential and the density moment from the ESA during intervals without cold plasma and radiation belt contamination (see panels (b) in Figure 1 and Figure S4). However, this estimate works for the plasma sheet region, where the ESA data set is reliable. In contrast, we may not provide the same estimate for the regions with a significant population of cold (<3 eV) electrons or high spacecraft potential. Note that Pedersen et al. (2008) estimated the uncertainties for a wide range of plasma parameters, showing that the uncertainties of this method may reach 100% under some conditions. It is important to carefully check these uncertainties before applying this method to analyze density-based parameters in EMIC wave interactions with charged particles, as they are crucial for accurately interpreting the results.

The ion temperature was derived from ESA measurements. We should note that the hot ion population beyond the ESA energy range (>30 keV) may contribute to the temperature for events with sufficiently hot ions. To verify this contribution, we evaluated the temperature from the combined measurements of ESA and the solid state telescope (SST; >50 keV) (Angelopoulos et al., 2008): THEMIS data set includes temperatures evaluated with merged ESA and SST spectra, including the interpolation of the $30 - 50$ keV region (see details in Runov et al., 2015; Turner et al., 2012). Comparison of the temperatures derived from ESA and from combined ESA and SST measurements (see Figure 2 in Artemyev et al., 2021, for details of such comparison) shows that the temperature based on ESA underestimates the actual temperature less than 30%. For most events, this underestimate is less than 20%. Therefore, in this study, we use the ion temperature derived from ESA measurements.

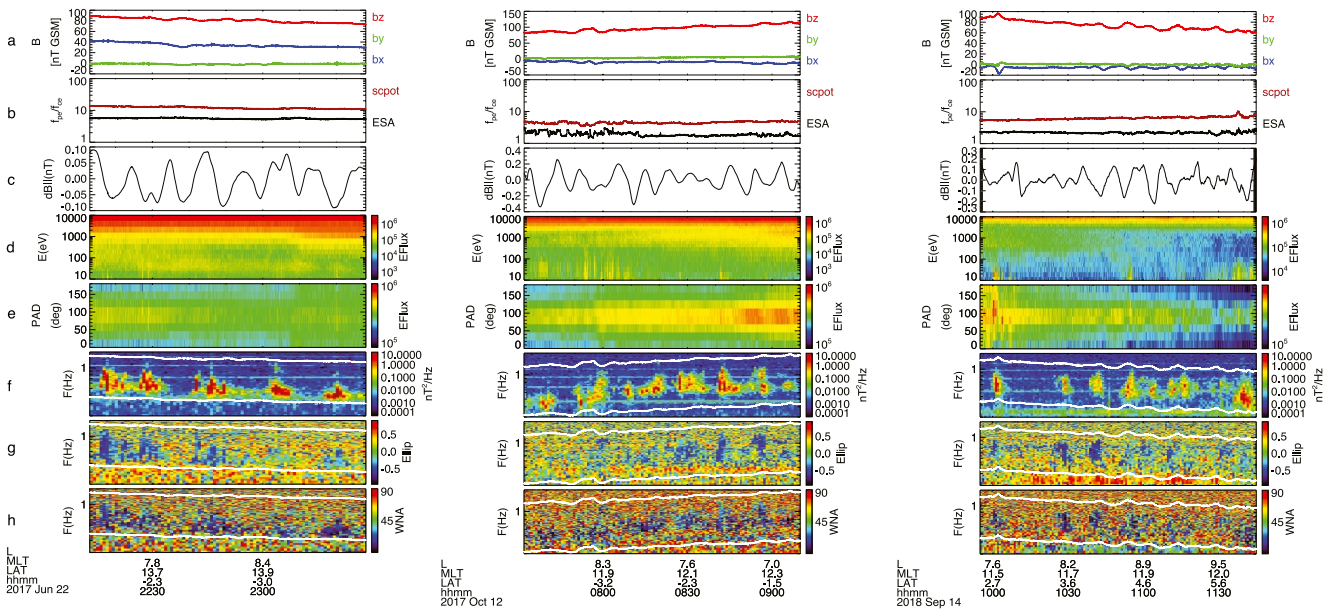

Figure 1. Three example events (22 June 2017 from THEMIS-A, & 12 October 2017 and 14 September 2018 from THEMIS-E) with quasi-periodic EMIC waves: (a) magnetic field components in GSM coordinates, (b) f_{pe}/f_{ce} ratio using spacecraft potential (red) and ESA measurements (black), (c) ultra-low frequency $\delta B_{\parallel}$ field, (d) omni-directional spectrum of ions, (e) pitch-angle distribution (f) EMIC wave magnetic field spectrum with overplotted white lines of cyclotron frequency of proton (f_{cp}) and Helium (f_{cHe}), (g) EMIC wave ellipticity, (h) EMIC wave normal angle.

For our statistical analysis, we have used 5 years of data from THEMIS-E and our event selection criteria include: (a) search for quasi-periodic EMIC waves with at least three wave intensity peaks within 1 hr, (b) determine the ULF wave frequency range (within $[0.1, 20]$ mHz) exhibiting good correlation between ULF magnetic field minima and EMIC wave intensity peaks. Only events exhibiting such correlations are included in the data set. Note that EMIC waves in Earth's magnetosphere are observed in different bands depending on the existence of hot and cold heavy ions and are most often characterized into the H^+, He^+ and O^+ bands (Chen, Zhu, & Zhang, 2019; Engebretson et al., 2018; Jun et al., 2021; Sigsbee et al., 2023). There has also been increased interest in studying EMIC waves in additional bands created by the presence of minor ions, including N^+ (Bashir & Ilie, 2018, 2021), He^{++} (Engebretson et al., 2018; Lee et al., 2019; Miyoshi et al., 2019), and O^{++} (Yu et al., 2021). However, in this study, we consider only H-band EMIC waves with frequency range $f \in [f_{cp}/4, f_{cp}]$, where f_{cp} is the proton gyrofrequency. Note that some of the H-band EMIC waves that we observe may also contain waves in the He^{++} band in the frequency range $f \in [f_{cp}/2, f_{cp}/4]$. This is possible because THEMIS can also sample EMIC waves in magnetospheric regions where solar wind entry can supply He^{++} ions and the instability threshold conditions for generating the He^{++} band waves are satisfied (Lee et al., 2019). This choice of considering H-band may be justified by the fact that (a) most of the events of ULF-modulated EMIC waves belong to a large L-shell dayside magnetosphere, where populations of cold plasmaspheric heavy ions are small and (b) studying the heavy ions band is beyond the scope of this paper, mainly because the THEMIS ESA instrument cannot resolve the heavy ions, especially hot ions (a previous work attempted to use the THEMIS ESA to resolve the presence of cold heavy ions (J. H. Lee & Angelopoulos, 2014)), and limit our ability to justify the existence of heavy ions and necessary threshold conditions. However, we plan to perform a comprehensive statistical study in the future for the occurrence of ULF-wave modulated EMIC waves including other EMIC wave bands (i.e., He^+, O^+, & He^{++}) utilizing wave and plasma measurements from missions equipped by mass spectrometers (e.g., Magnetospheric Multiscale Mission (Burch et al., 2016; Young et al., 2016) and Cluster (Escoubet et al., 2001; Rème et al., 2001)) capable of measuring those ions in wide energy range in the magnetosphere.

Figure 1 shows three typical events from the data set collected. All are from the near-equatorial (B_z is the dominant component; see Panels (a)) transition region between the plasma sheet and the inner magnetosphere. The electron plasma frequency to electron gyrofrequency ratio, $f_{pe}/f_{ce} \in [5, 10]$, is typical for the near-Earth plasma sheet (see Panels (b)). Note that f_{pe}/f_{ce} derived from the spacecraft-potential density is much larger

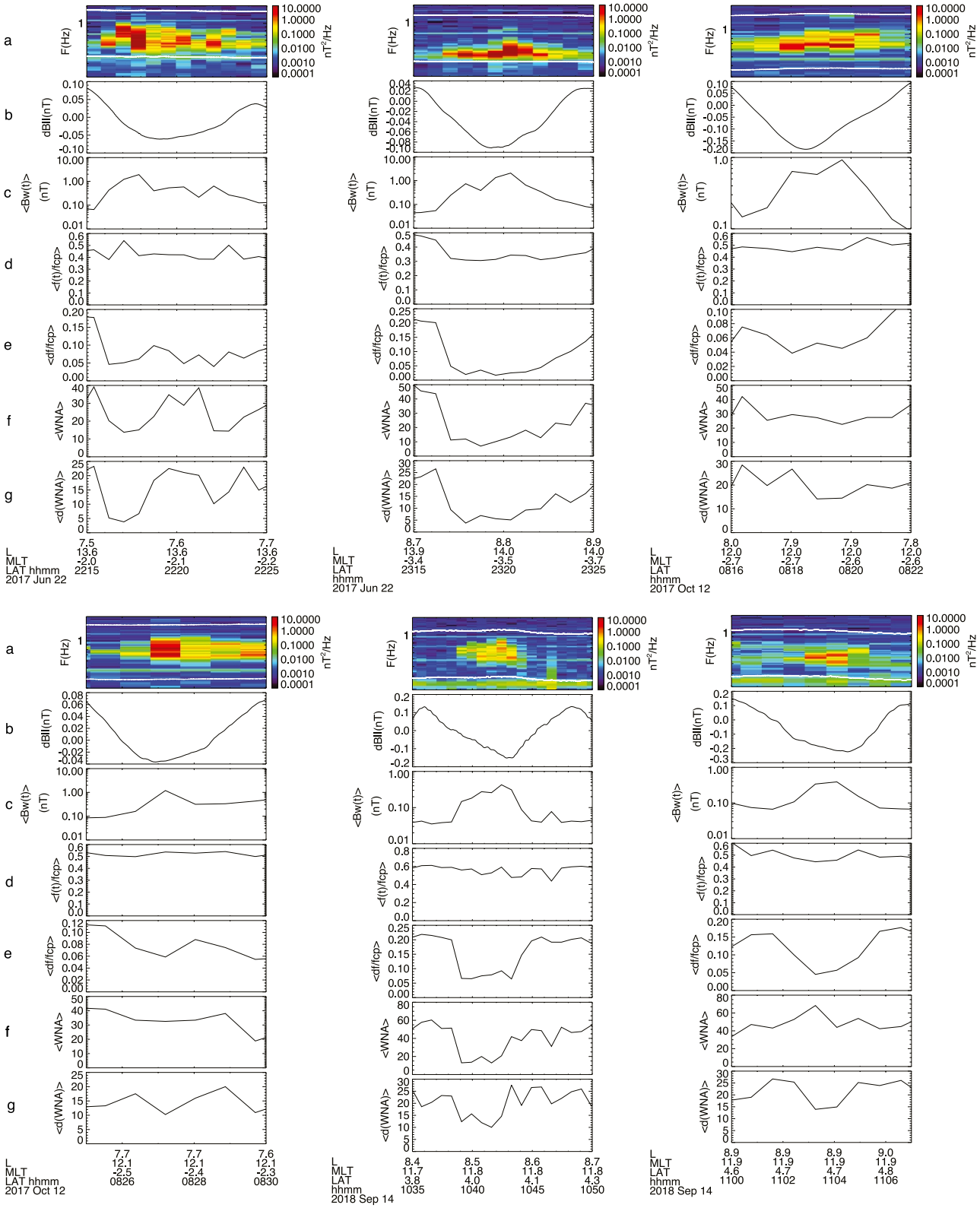

Figure 2. Characteristics of individual EMIC wave bursts associated with local $\delta B_{\parallel}$ minima for three events from Figure 1: (a) EMIC wave power spectral density $\mathcal{B}_w^2\left(nT^2/Hz\right)$ (same as panel (f) in Figure 1), (b) ultra-low frequency field minima, (c) EMIC wave amplitude $<\mathcal{B}_w(t)> = \sqrt{<\mathcal{B}_w^2(t)>}$, (d) EMIC wave mean frequency normalized to f_{cp}, (e) width of EMIC wave mean frequency normalized to f_{cp}, (f) EMIC wave mean wave normal angle, and (g) width of the wave normal angle distribution.

than f_{pe}/f_{ce} based on ESA density measurements, because a significant fraction of cold electrons is not measured by the ESA (McFadden et al., 2008).

Using magnetic field measurements, B, we evaluate compressional fluctuations in the ULF frequency range: $\delta B_{\parallel} = (B - \langle B \rangle) \cdot \langle B \rangle / |\langle B \rangle|$. Panels (c) show quasi-periodic $\delta B_{\parallel}$ variations with amplitudes of a fraction of nT, that is, $\delta B_{\parallel}/|\langle B \rangle| \sim 10^{-3}$. To evaluate $\delta B_{\parallel}$, we use the frequency range $[0.1, 20]$ mHz (i.e., $\delta B_{\parallel} = (B - \langle B \rangle) \cdot \langle B \rangle / |\langle B \rangle|$ denotes the averaging of 7 min). For each event, we additionally check if changing the lower and upper-frequency limits (within the $[0.1, 20]$ mHz range) may improve the $\delta B_{\parallel}$ correlation with the EMIC wave intensity, and adjust these limits to maximize this correlation. Such compressional ULF waves propagate in a hot, transversely anisotropic ion background (see Panels (d, e)), and even with their low amplitude can drive EMIC wave generation (see details in Shahid et al., 2024). Fast Fourier Transform (FFT) analysis is used to identify EMIC waves and minimum variance analysis for quantitative determination of the wave ellipticity and wave normal angle. Panels (f) show quasi-periodic EMIC wave bursts correlated with local minima of $\delta B_{\parallel}$, which are usually associated with an enhanced hot transversely anisotropic ion population contributing to the pressure balance (e.g., Balikhin et al., 2009; Soto-Chavez et al., 2019). Although EMIC waves may also be associated with $\delta B_{\parallel}$ maxima (see Loto'Aniu et al., 2009), our statistics include only EMIC wave bursts embedded in $\delta B_{\parallel}$ minima. Wave ellipticity and polarization (panels (g, h)) confirm that these are classical, field-aligned EMIC waves. These wave properties are estimated using the MVA technique (Sonnerup & Scheible, 2000). Note that although we determine polarization and ellipticity for each wave burst, we do not use these properties for event selection.

Figure 2 zooms in on several EMIC wave bursts from Figure 1. All bursts are associated with local minima of ULF $\delta B_{\parallel}$, and such a type of correlation has been found for all events in our data set. The mean wave intensity $\langle \mathcal{B}_w^2(t) \rangle = \int_{f_{cp}/4}^{f_{cp}} \mathcal{B}_w^2(t, f) df$ giving the wave amplitude ($<\mathcal{B}_w(t)> = \sqrt{<\mathcal{B}_w^2(t)>}$) about $0.2 - 1$ nT and the mean wave frequency $\langle f(t) \rangle = \frac{1}{\langle B_w^2(t) \rangle} \int_{f_{cp}/4}^{f_{cp}} f \mathcal{B}_w^2(t, f) df$ is about $0.2 - 0.4 f_{cp}$, quite typical for EMIC waves in the inner magnetosphere (see, e.g., Kersten et al., 2014; Zhang et al., 2016). For each wave burst, we also calculate the wave frequency variance $<df^2(t)> = \frac{1}{\langle B_w^2(t) \rangle} \int_{f_{cp}/4}^{f_{cp}} (f - \langle f(t) \rangle)^2 \mathcal{B}_w^2(t, f) df$ averaged over the burst interval giving the wave frequency width $df(t) = \sqrt{<df^2(t)>}$, the mean wave normal angle WNA, and the dispersion of wave normal angles, $dWNA$ (both are obtained by the MVA technique (Sonnerup & Scheible, 2000) and averaged over the wave burst interval same as frequency). The wave bursts shown in Figure 2 are quite narrow-banded with $df(t)/\langle f(t) \rangle < 1/5$ and weakly oblique with $WNA \approx 20° \pm 10°$. Some of the EMIC waves have linear polarization and oblique wave normal angles. Not all of the bursts shown are consistent with "classic" field-aligned, left-hand circularly polarized EMIC waves. We determine these characteristics for all wave bursts in our data set.

Although the correlation between ULF waves and EMIC wave bursts is well seen in examples shown in Figures 1 and 2 (each EMIC burst can be associated with a local minimum of the ULF field), this correlation cannot be quantified by the correlation coefficient, because both ULF and EMIC wave amplitude signals contain multiple frequency bands. The magnitude of EMIC wave bursts and ULF minima vary within the event, and this radically reduces the directly calculated correlation coefficient. Therefore, we collect a data set of our events using the alternative approach. For each event, we plot spectra of ULF wave and EMIC wave amplitudes, and select only events showing the main spectra peak in the same frequency (despite such spectra can contain multiple additional peaks corresponding to ULF and EMIC amplitude variations from one minimum (burst) to another one (see examples in Figure 2)). We then visually check that for all selected events each burst of EMIC waves is associated with a local minimum of $\delta B_{\parallel}$ (more than 20% reduction of $\delta B_{\parallel}$).

Figure 3 shows the histograms for the L-shell and MLT distributions for all data sets: ULF-modulated EMIC waves are mostly observed at high L-shells ($L > 8$) at the dayside sector (from 10 to 16), where compressional ULF waves are predominantly observed in response to solar wind transients and magnetopause oscillations (M. Hartinger et al., 2011; M. D. Hartinger et al., 2013; Wang et al., 2018; Wang, Nishimura, et al., 2019). At dawn and dusk flanks, ULF-modulated EMIC waves are only observed at high L, whereas at the dayside such waves can be found even at $L \sim 5 - 6$. Note that in the text we use dawn/day/dusk MLT sectors for $MLT \in [0, 8]$, $[8, 14]$, and $[14, 24]$. In Figure 3, at $L \sim 5$ the number of events is quite small on this grid and is statistically insignificant. That's why for our statistical results in Figures 5–7, especially for comparison of observed and fitted parameters,

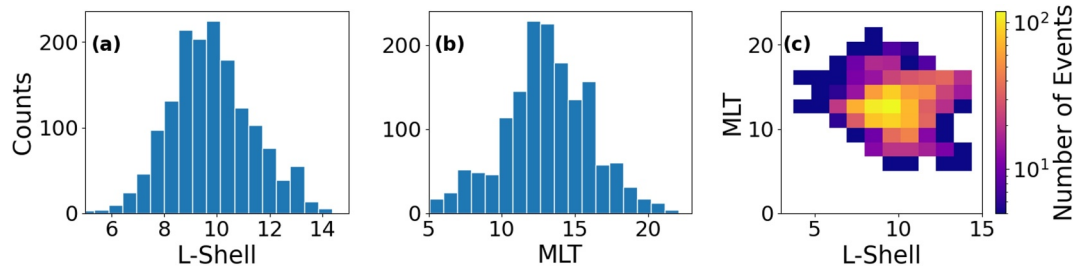

Figure 3. Distribution of events (individual EMIC wave bursts associated with ultra-low frequency $\delta B_{\parallel}$ minimum): (a) *L*-shell distribution, (b) *MLT* distribution, and (c) distribution of the total number of events in (*L*, *MLT*) plane.

we use only bins with at least 5 events. We have also provided the results without limiting them to five events in Figures S1–S3.

3. Statistical Properties of ULF-Modulated EMIC Waves

Figure 4 shows the distributions of the statistical properties of the ULF-modulated EMIC waves. Burst-averaged wave amplitude (square root of the average wave intensity) is usually within [50, 500] pT, but there are rare observations of very intense (~1nT) waves (see panel (a)). Amplitudes of [50, 500] pT are typical for the inner magnetosphere EMIC waves (Jun et al., 2019; Zhang et al., 2016). f_{pe}/f_{ce} in panel (b) is the maximum value during each ULF-Modulated EMIC wave burst. Contrast to EMIC waves observed in the inner magnetosphere around plasma plumes with large f_{pe}/f_{ce} (see Halford et al., 2015; Usanova et al., 2013), ULF-modulated EMIC waves in our statistics are mostly observed in a quite rarefied plasma environment with $f_{pe}/f_{ce} < 10$ (see panel (b)), typical in the plasma sheet. As f_{pe}/f_{ce} controls the electron resonant energies for EMIC waves, small $f_{pe}/f_{ce} < 10$ would not allow EMIC waves to scatter ≤1 MeV electrons (Summers & Thorne, 2003), and only a small population of observations with $f_{pe}/f_{ce} > 15$ can explain the precipitation of ≤1 MeV electrons.

Most ULF-modulated EMIC waves are moderately oblique with $WNA \in [30°, 60°]$, with quite a small variation of wave normal angle, $dWNA \sim 7°$ (see panels (c, d)). Such an obliqueness may affect relativistic electron scattering by EMIC waves (Gamayunov & Khazanov, 2007; Khazanov & Gamayunov, 2007) and should be quite

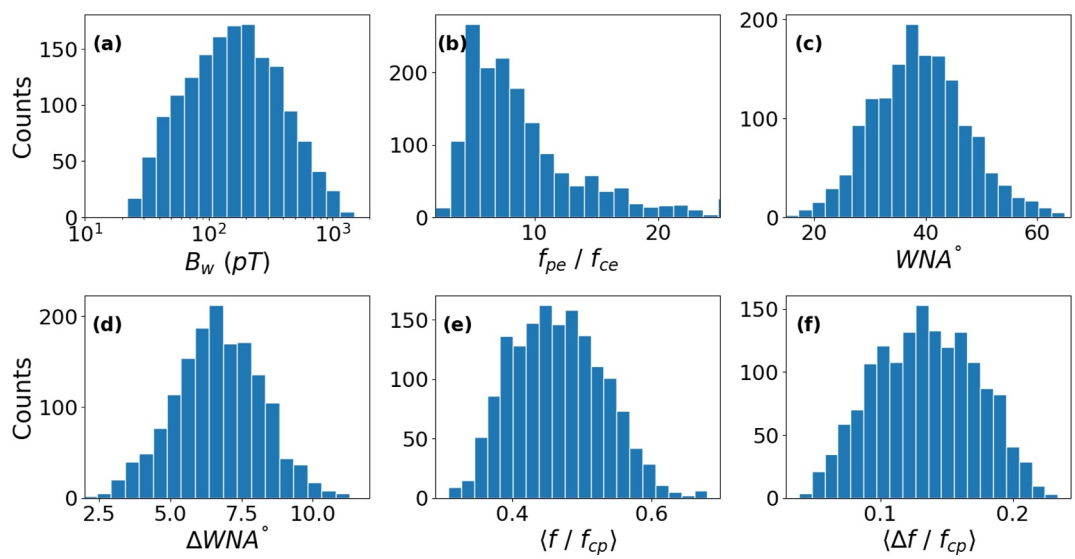

Figure 4. (a) Distributions of EMIC wave amplitudes $\langle B_w \rangle$, (b) f_{pe}/f_{ce} ratio from spacecraft potential, (c) mean wave normal angle, (d) width of the wave normal angle distribution, (e) mean wave frequency $\langle f/f_{cp} \rangle$, and (f) wave frequency width $\langle \Delta f/f_{cp} \rangle$.

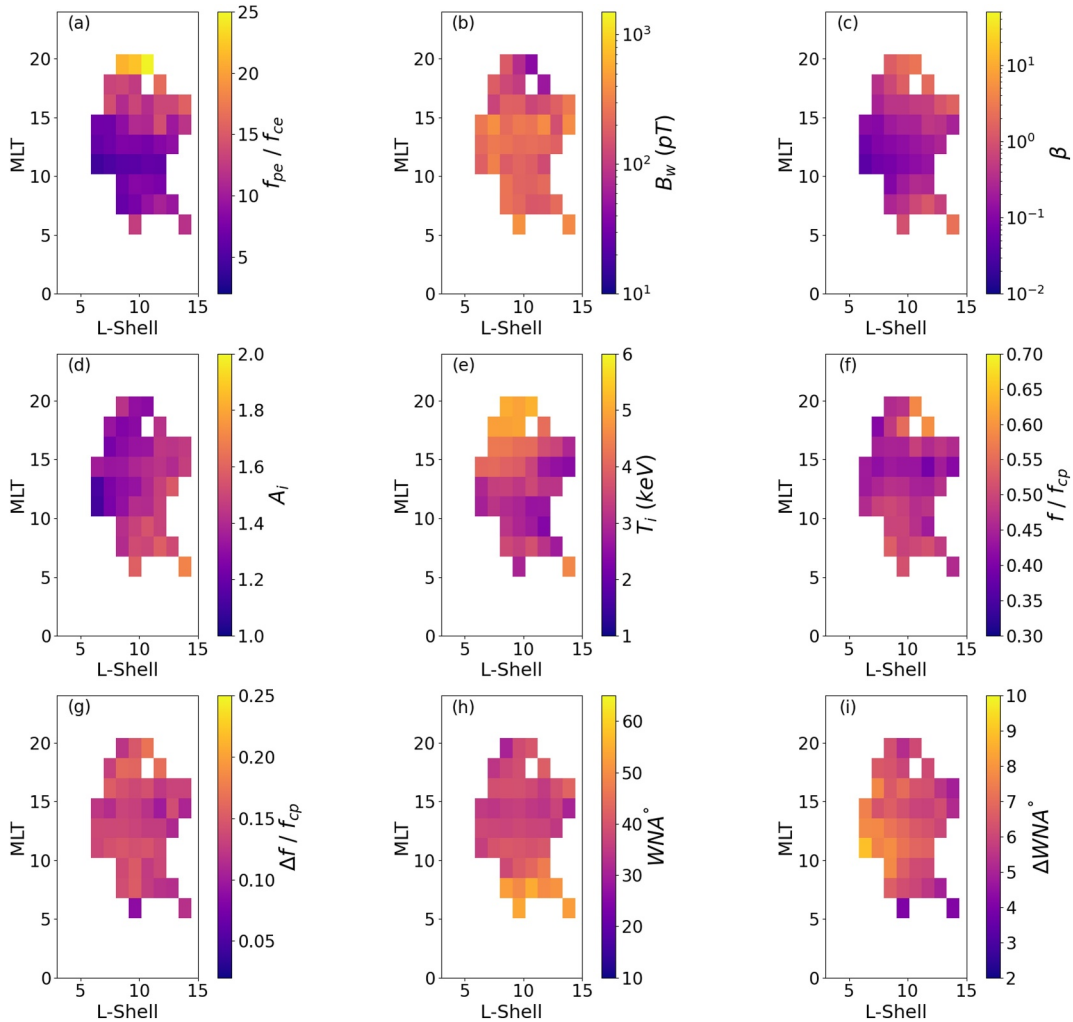

Figure 5. Distributions of main wave characteristics from Figure 4 in (L, MLT) plane. (a) f_{pe}/f_{ce} from spacecraft potential, (b) wave amplitude B_w, (c) ion plasma β_i, (d) temperature anisotropy, (e) ion temperature from ESA measurements in keV, (f) normalized wave frequency, (g) normalized width of wave frequency, (h) wave normal angle, (i) width of wave normal angle. Note that<...> is omitted for simplicity for all parameters.

important for EMIC wave Landau resonance with warm electrons (Fu et al., 2018; Inaba et al., 2021; Wang, Li et al., 2019) and plasma sheet ions (Ma et al., 2019; Usanova, 2021). The observed ULF-modulated EMIC wave frequencies and frequency widths, $<f/f_{cp}> \in [0.4, 0.55]$ and $<\Delta f/f_{cp}> \in [0.1, 0.2]$ (see panels (e, f) and note that $df(t) = \Delta f(t)$), are typical for EMIC waves in the inner magnetosphere (Kersten et al., 2014; Zhang et al., 2016).

Figure 5 shows the spatial distribution of all the wave and background plasma/magnetic field characteristics. There is a clear dawn-dusk asymmetry of f_{pe}/f_{ce} and ion temperature T_i calculated from the ESA instrument for ULF-modulated EMIC events: f_{pe}/f_{ce} is approximately 10 at the dawn flank and increases to 20 at the dusk flank; T_i is about 3 keV at the dawn flank and increases to 5 keV at the dusk flank. These results are consistent with the general statistics from the Cluster observation of f_{pe}/f_{ce} associated with EMIC waves (Allanson et al., 2016), that is, ULF-modulated EMIC waves and EMIC waves not associated with ULF waves are observed under the same plasma conditions.

The root mean square amplitude is slightly larger on the dawn flank, $\langle B_w \rangle \sim 200$ pT, than on the dusk flank, $\langle B_w \rangle \sim 50$ pT. Ion $\beta_i = 8\pi n T_i / B_0^2$ maximizes at flanks, $\beta_i \sim 10$, and has a minimum on the dayside and at low

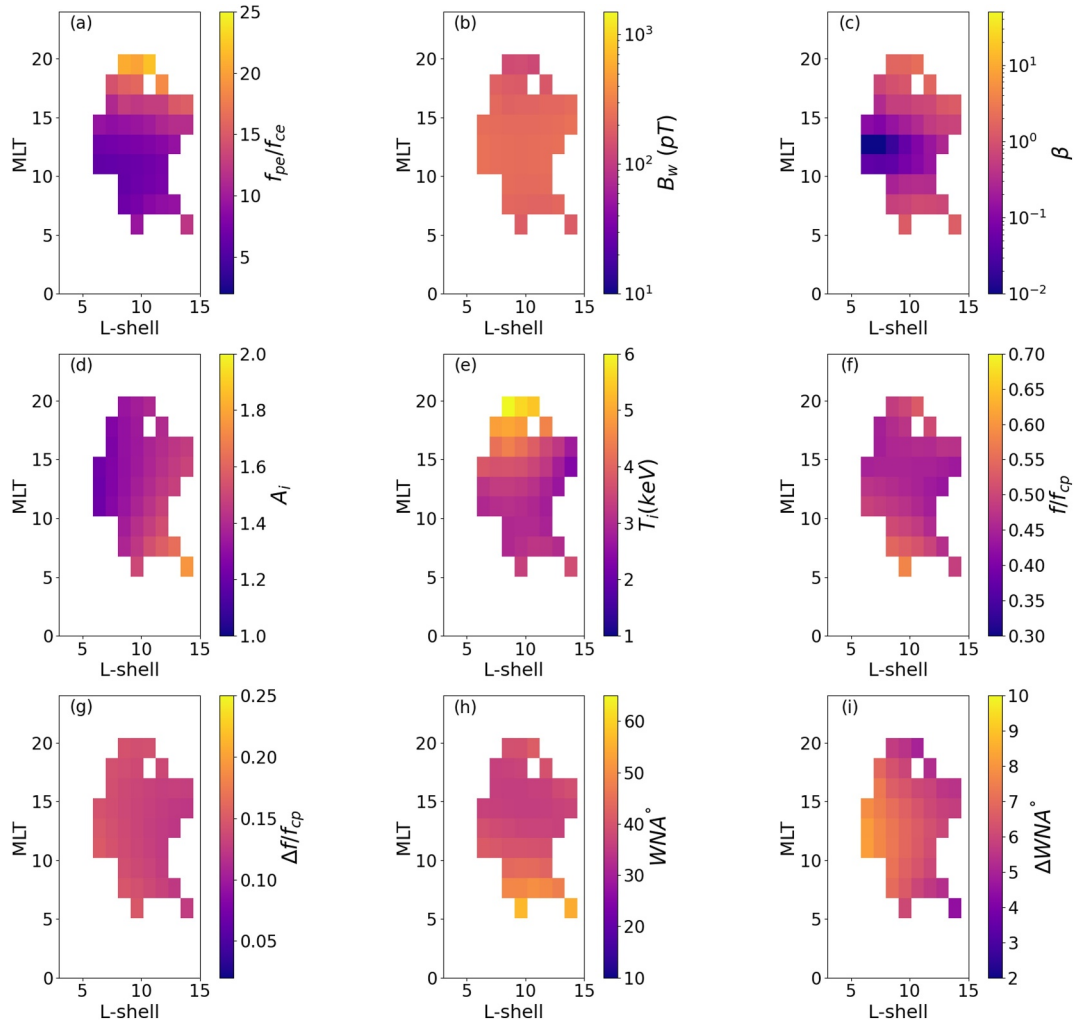

Figure 6. Distributions of main wave characteristics same as Figure 5 in (L, MLT) plane but using the empirical model (Equation 1) and coefficients (Table 1) obtained from fits.

L, and $\beta_i < 1$. Ion temperature anisotropy, the key parameter for wave generation, has a maximum at dawn flank, $A_i = T_{i,\perp}/T_{i,\parallel} \sim 1.6$; this is consistent with generally more anisotropic ion populations associated with EMIC wave observations in noon/dawn flank (see Anderson et al., 1992; J. H. Lee & Angelopoulos, 2014; Min et al., 2012). This peak of A_i most likely explains the dawn flank peak of $\langle B_w \rangle$. Note that although ULF wave amplitudes may have some MLT dependence, for our data set of ULF-modulated EMIC waves, the observed ULF amplitudes do not show any maximum at the dawn flank. Therefore, variations of the EMIC wave properties should be associated with the local plasma parameters. The maximum anisotropy on the dawn flank cannot be associated with plasma sheet injections, because the injected ions drift at the dusk flank, where most of the anisotropy is released for the generation of EMIC waves (Jun et al., 2019, 2021). Therefore, Figure 5d likely shows the selection effect: dawn flank is characterized by lower f_{pe}/f_{ce} ratio, and thus resonant ion energies are higher and fluxes are lower for EMIC wave generation; this implies that a higher level of anisotropy is required for the generation of EMIC waves at dawn flank.

Panels (h–l) in Figure 5 show the distribution of the main wave characteristics. The mean wave frequency $<f/f_{cp}>$ and the frequency width df/f_{cp} do not vary much with MLT: for example, there is only a slightly lower $<f/f_{cp}> \approx 0.4$ on the dusk flank, in comparison with $<f/f_{cp}> \approx 0.5$ on the dawn side. However, there is a clear gradient of wave normal angle with MLT: waves at the dusk flank are more field-aligned with $WNA \approx 35°$ than in the dawn flank, where $WNA \approx 55°$. This is consistent with the general THEMIS statistics of EMIC waves (Min et al., 2012), that is, WNA is likely dictated by local properties of hot ion populations responsible for EMIC wave

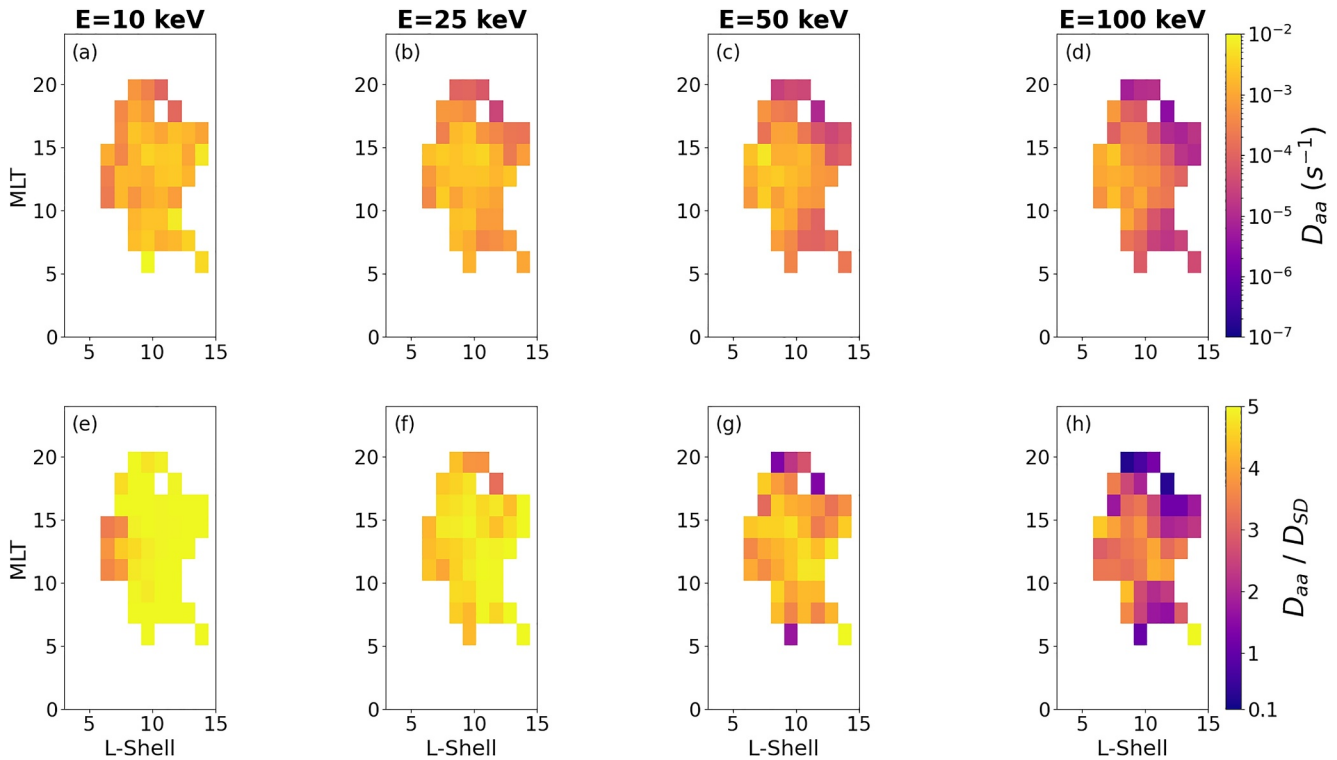

Figure 7. Distribution of pitch-angle diffusion coefficients in (L, MLT) plane at $E = (10, 25, 50, 100)$ keV (a–d) $D_{\alpha\alpha}$ distribution (e–h) $D_{\alpha\alpha}/D_{\mathrm{SD}}$ distribution.

generation and does not depend on ULF-modulation (see also discussion in Anderson et al., 1992). Interestingly, the wave normal angle variation, $dWNA$, does not depend on MLT, but increases at lower L-shells, from $dWNA \sim 5°$ at $L \sim 12$ to $dWNA \sim 10°$ at $L \sim 5$.

4. Empirical Model

Distributions of the main wave characteristics shown in Figure 5 can be used to estimate the ion diffusion rates that would describe plasma sheet and ring current ion precipitation via resonant scattering by ULF-modulated EMIC waves. To enable the evaluation of diffusion rates, we develop emprical model for the ULF-Modulated EMIC wave properties (wave amplitude $<B_w>$, mean wave frequency $<f/f_{cp}>$, and frequency distribution width $<\Delta f/f_{cp}>$, wave normal angle WNA, and its width dWNA, and the plasma parameters (plasma-to-electron cyclotron frequency ratio, from ESA $f_{pe}(ESA)/f_{ce}$ and spacecraft potential f_{pe}/f_{ce}, Ion plasma beta β_i, ion temperature anisotropy A_i) as a function of MLT and L as.

$$F(a_{i=0,5},\ L,\ MLT) = a_0 + a_1 \cdot (L/10) + a_2 \cdot MLT + a_3 \cdot (L/10) \cdot MLT + a_4 \cdot (L/10)^2 \cdot MLT + a_5 \cdot (L/10) \cdot MLT^2 \quad (1)$$

that capture main L and MLT gradients of wave characteristics. Note that these empirical model only works within the region of ULF-modulated EMIC wave observations: $MLT \in [5, 20]$, $L \in [5, 12]$, with two boundaries $MLT_- = 15 - L$ and $MLT_+ = 10 + L$. The fitting parameters a_i, $i = 0$ to 5 are obtained using the non-linear least-squares fitting method. Table 1 shows the coefficients of these empirical model for each quantity. We also present the statistical properties in Figure 6 using our empirical model and coefficients given in Table 1. The results obtained from the empirical model agree well with the parameters observed in Figure 5.

5. Estimation of Pitch Angle Diffusion Rate

We use the empirical model for the observed EMIC wave characteristics and plasma parameters (i.e., f_{pe}/f_{ce} from spacecraft potential) to quantify wave contribution to plasma sheet and ring current ion losses. This was done by

Table 1
Empirical Model (See Equation 1) Coefficients for EMIC Wave Characteristics, and Plasma Parameters ($f_{pe}(ESA)/f_{ce}$ From ESA Measurement, f_{pe}/f_{ce} From Spacecraft Potential, Ion Temperature (T_i) and Anisotropy (A_i) From ESA Measurement, and Ion Beta β_i (Density From Spacecraft Potential and Temperature From ESA Measurement))

Parameters (F)	a_0	a_1	a_2	a_3	a_4	a_5
$f_{pe}(ESA)/f_{ce}$	5.46	11.11	0.15	−3.24	1.04	0.08
f_{pe}/f_{ce}	−2.32	22.79	0.75	−3.72	0.26	0.13
B_w(pT)	0.26	−0.21	0.01	0.00	0.01	0.00
β_i	1.22	2.83	−0.05	−0.67	0.07	0.02
A_i	0.67	1.05	0.00	0.03	−0.01	0.00
T_i(keV)	−0.25	5.44	0.03	−0.13	−0.34	0.02
f/f_{cp}	0.94	−0.18	−0.03	0.00	0.00	0.00
$\Delta f/f_{cp}$	0.22	−0.05	0.00	0.00	0.00	0.00
$WNA°$	67.06	16.19	−1.16	−5.88	0.93	0.19
$dWNA°$	11.83	−8.00	0.06	0.22	0.19	−0.02

parametrizing the wave characteristics so that they can be applied to evaluate how efficiently these waves contribute to the pitch angle diffusion of the energetic ions.

We use a simplified formula by assuming the waves as field-aligned, although some of them are weakly oblique (see Summers et al., 2007, for equations of diffusion coefficients in the quasi-linear theory):

$$D_{\alpha\alpha} = \frac{\pi}{2}\frac{1}{\nu}\frac{\Omega_{cp}^2}{|\Omega_{ce}|}\frac{1}{(E+1)^2}\frac{R\left(1-\frac{x\cos\alpha}{y\beta_E}\right)^2|F(x,y)|}{\delta x|\beta_E\cos\alpha - F(x,y)|}e^{-\left(\frac{x-x_m}{\delta x}\right)^2}$$

Here $\nu = \sqrt{\pi}\,erf(\sigma)$, and erf is the error function with $\sigma = 4/3$ for ions, c is the speed of light in vacuum, $\Omega_{cp} = 2\pi f_{cp}$, $\Omega_{ce} = 2\pi f_{ce}$ that is, $f_{cp} = e|B_0|/m_p c$ and $f_{ce} = e|B_0|/m_e c$ are the proton cyclotron and electron cyclotron frequencies, m_e and m_p are the rest masses of the electrons and proton, and e is the unit charge. Also, $x = f/f_{cp}$, $y = kc/2\pi f_{cp}$, E is the dimensionless particle kinetic energy given by $E = E_k/(m_i c^2) = \gamma - 1$, $\beta_E = [E(E+2)]^{1/2}/(E+1)$. $R = B_w^2/B_0^2$ is the ratio of the energy density of the wave magnetic field to that of the background field, that is, the relative wave power; $x_m = <f_m/f_{cp}>(= 0.35$ is fixed), $\delta x = \Delta f/f_{cp}$ and f_{pe}/f_{ce} are used from observed statistics. x, y, $F(x,y) = dx/dy$ are determined from the cold plasma dispersion of EMIC waves (Stix, 1962). The diffusion rate $D_{\alpha\alpha}$ evaluated at the loss-cone pitch-angle, $\alpha_{LC}(L)$, determines the rate of wave-driven ion precipitation into the atmosphere (Kennel & Petschek, 1966). This diffusion rate can be compared to the so-called strong diffusion rate (Summers & Thorne, 2003)

$$D_{\rm SD} = \frac{9.66}{L^4}\left[\frac{4L}{4L-3}\right]^{1/2}\frac{[E(E+2)]^{1/2}}{(E+1)}$$

that determines the maximum possible precipitation rate in the diffusion regime (Kennel, 1969; Kennel & Petschek, 1966). Although a significant fraction of ULF-modulated EMIC bursts are observed within the plasma sheet, where ion β approaches one or can be large (see Figure 5c), for statistical evaluation of diffusion rates we use cold plasma dispersion relation. The hot plasma effects are known to change the resonant energies for EMIC wave interaction with electrons (e.g., Bashir et al., 2022; H. Chen, Gao, Lu, & Wang, 2019; Ni et al., 2018), and in the next studies these effects should be investigated for EMIC wave-ion resonances as well. The same comment is valid for our assumption of field-aligned wave propagation: the observed non-zero *WNA* indicates that the obliquity should be included in the further investigation of efficiency of ULF-modulated EMIC waves (see Gamayunov & Khazanov, 2007; D.-Y. Lee et al., 2018, for discussion how wave obliquity modifies the efficiency of relativistic electron scattering by EMIC waves).

Figure 7 shows the diffusion rates $D_{\alpha\alpha}$ and $D_{\alpha\alpha}/D_{\rm SD}$ at four ion energies and $\alpha_{LC}(L)$. At $MLT \in [5,15]$ and $L > 10$, ULF-modulated EMIC waves provide very strong $D_{\alpha\alpha} \sim 10^{-2}\mathrm{s}^{-1}$, above the strong diffusion limit ($D_{\alpha\alpha}/D_{\rm SD} > 1$). Thus, when these waves are present (i.e., when sufficiently strong ULF waves transport hot anisotropic ions and EMIC waves), they will drive the modulated ion (proton) losses for a wide energy range. Such losses can be observed as day-side proton aurora forms (e.g., Berchem et al., 2003; Lorentzen & Moen, 2000; Sigernes et al., 1996), and some of these forms are indeed observed poleward from the proton aurora oval, that is, within the plasma sheet (see review by Frey, 2007). One such form, that may be associated with EMIC wave-driven precipitations of ions near the magnetopause, where ULF waves are driven by solar wind transients and can modulate EMIC waves, is so called High-Latitude Dayside Aurora (e.g., Murphree et al., 1990). Sub-auroral day-side proton precipitations (equatorward from the auroral oval) also may have transient character and be driven by EMIC waves (Fuselier et al., 2004). Although such transient proton precipitations can be potentially driven by ULF-modulated EMIC waves, their L-shells are lower than the main statistics of our data set (see Figure 3a), and further investigation of low L-shell ULF-modulation of EMIC waves is needed to connect this wave activity with sub-auroral proton precipitations.

6. Discussion and Conclusions

In this study, we examine a specific class of EMIC waves modulated by compressional ULF waves. The likely scenario for such EMIC wave generation includes the day-side magnetopause impact by solar wind transients that drive compressional ULF waves (presumably drift mirror mode waves Balikhin et al., 2009; Cooper et al., 2021; Rae et al., 2007; Soto-Chavez et al., 2019), and these ULF waves transport the hot, transversely anisotropic ion population to lower L-shells, where the ion anisotropy is released in the form of EMIC wave generation (see examples in Kitamura et al., 2021; Loto'Aniu et al., 2009; Z. Y. Liu et al., 2022; Yin et al., 2022). This scenario is confirmed by the prevalence of ULF-modulated EMIC waves at large L-shells ($L \in [8, 12]$) on the day-side $MLT \in [10, 16]$. Therefore, we may suggest that such ULF-modulated EMIC waves constitute an additional class of EMIC waves, supplementing the two most investigated classes: EMIC waves generated on the dusk flank by plasma sheet-injected ions and EMIC waves generated at low L-shells on the day-side by compressionally heated ions (e.g., Jun et al., 2019, 2021; N. Liu et al., 2022; Xue et al., 2022). The main feature of this new EMIC wave class is the periodicity of EMIC emission.

These ULF-modulated EMIC waves are moderately oblique ($WNA \in [30°, 60°]$), quite narrow-banded ($\Delta f/f \sim 0.3$ with $f/f_{cp} \in [0.4, 0.55]$), and moderately intense ($B_w \in [50, 300]$ pT). Due to their insufficiently high wave amplitudes, these waves resonate with protons in the quasi-linear regime. The main ion population responsible for the generation of ULF-modulated EMIC waves is typical plasmasheet ions with energies $E_R \in [5, 15]$ keV. Due to the relatively small plasma density at high L, the frequency ratio f_{pe}/f_{ce} during ULF-modulated EMIC waves is about $\in [5, 10]$. This ratio controls the resonant energies for electrons interacting with EMIC waves, and when $f_{pe}/f_{ce} \in [5, 10]$ EMIC waves cannot scatter relativistic or energetic electrons, but only ultra-relativistic electrons that are usually scarce in such high L-shells. Therefore, ULF-modulated EMIC waves are not effective in driving electron losses. However, these waves are very effective in scattering ions (pitch-angle diffusion rate reaches the strong diffusion limit for [10, 100] keV ions). Therefore, ULF-modulated EMIC waves can produce quasiperiodic ion precipitation that contributes to the day-side proton aurora (Berchem et al., 2003; Frey, 2007; Lorentzen & Moen, 2000; Sigernes et al., 1996). Further transported by ULF waves to lower L-shells, hot anisotropic ion population may generate EMIC waves within the outer radiation belt, where these waves are expected to serve as the seed population for intense coherent EMIC waves (see discussions in Gamayunov & Engebretson, 2021, 2022).

Statistics of ULF-modulated EMIC waves demonstrate one more mechanism of direct solar wind impact on the Earth's magnetosphere (see discussions of other mechanisms in M. D. Hartinger et al., 2013; M. D. Hartinger et al., 2014; Wang et al., 2018; Wang, Nishimura, et al., 2019), which underlines the importance of including solar wind transients into models of inner magnetosphere dynamics and magnetosphere-ionosphere coupling.

Data Availability Statement

THEMIS data is available at http://themis.ssl.berkeley.edu. Data access and processing were performed using the space physics environment data analysis system (SPEDAS), see Angelopoulos et al. (2019).

Acknowledgments
Work of M.F.B., A.A., X.-J. Z. are supported by NSF Grant 2329897, and NASA Grants 80NSSC20K1270, 80NSSC23K0403, 80NSSC23K0108. M. S. acknowledges support through Higher Education Commission of Pakistan's 6 month International Research Support Initiative Program (IRSIP) to visit UCLA, Prof. Vassilis Angelopoulos for additional funding during the Visit, and Salam Chair Research Fellowship. M.S. acknowledges Gohar Abbas (GC University Lahore) for his suggestions and discussions. We acknowledge the support of NASA contract NAS5-02099 for the use of data from the THEMIS Mission, specifically K. H.Glassmeier, U. Auster and W. Baumjohann for the use of FGM data (provided under the lead of the Technical University of Braunschweig and with financial support through the German Ministry for Economy and Technology and the German Center for Aviation and Space (DLR) under contract 50 OC 0302).

References

Allanson, O., Wilson, F., & Neukirch, T. (2016). Neutral and non-neutral collisionless plasma equilibria for twisted flux tubes: The Gold-Hoyle model in a background field. *Physics of Plasmas*, *23*(9), 092106. https://doi.org/10.1063/1.4962507

Anderson, B. J., Erlandson, R. E., & Zanetti, L. J. (1992). A statistical study of Pc 1-2 magnetic pulsations in the equatorial magnetosphere 2. Wave properties. *Journal of Geophysical Research*, *97*(A3), 3089–3101. https://doi.org/10.1029/91JA02697

Angelopoulos, V. (2008). The THEMIS mission. *Space Science Reviews*, *141*(1–4), 5–34. https://doi.org/10.1007/s11214-008-9336-1

Angelopoulos, V., Cruce, P., Drozdov, A., Grimes, E. W., Hatzigeorgiu, N., King, D. A., et al. (2019). The space physics environment data analysis system (SPEDAS) (version 6.0) [Software]. *Space Science Reviews*, *215*(1), 9. https://doi.org/10.1007/s11214-018-0576-4

Angelopoulos, V., Sibeck, D., Carlson, C. W., McFadden, J. P., Larson, D., Lin, R. P., et al. (2008). First results from the THEMIS mission. *Space Science Reviews*, *141*(1–4), 453–476. https://doi.org/10.1007/s11214-008-9378-4

Angelopoulos, V., Zhang, X. J., Artemyev, A. V., Mourenas, D., Tsai, E., Wilkins, C., et al. (2023). Energetic electron precipitation driven by electromagnetic ion cyclotron waves from ELFIN's low altitude perspective. *Space Science Reviews*, *219*(5), 37. https://doi.org/10.1007/s11214-023-00984-w

Artemyev, A. V., Lu, S., El-Alaoui, M., Lin, Y., Angelopoulos, V., Zhang, X.-J., et al. (2021). Configuration of the Earth's magnetotail current sheet. *Geophysical Research Letters*, *48*(6), e92153. https://doi.org/10.1029/2020GL092153

Auster, H. U., Glassmeier, K. H., Magnes, W., Aydogar, O., Baumjohann, W., Constantinescu, D., et al. (2008). The THEMIS fluxgate magnetometer. *Space Science Reviews*, *141*(1–4), 235–264. https://doi.org/10.1007/s11214-008-9365-9

Balikhin, M. A., Sagdeev, R. Z., Walker, S. N., Pokhotelov, O. A., Sibeck, D. G., Beloff, N., & Dudnikova, G. (2009). THEMIS observations of mirror structures: Magnetic holes and instability threshold. *Geophysical Research Letters*, *36*(3), 3105. https://doi.org/10.1029/2008GL036923

Bashir, M. F., Artemyev, A., Zhang, X.-J., & Angelopoulos, V. (2022a). Hot plasma effects on electron resonant scattering by electromagnetic ion cyclotron waves. *Geophysical Research Letters*, *49*(11), e99229. https://doi.org/10.1029/2022GL099229

Bashir, M. F., Artemyev, A., Zhang, X.-J., & Angelopoulos, V. (2022b). Energetic electron precipitation driven by the combined effect of ULF, EMIC, and whistler waves. *Journal of Geophysical Research: Space Physics*, *127*(1), e2021JA029871. https://doi.org/10.1029/2021ja029871

Bashir, M. F., & Ilie, R. (2018). A new N^+ band of electromagnetic ion cyclotron waves in multi-ion cold plasmas. *Geophysical Research Letters*, *45*(19), 10150–10159. https://doi.org/10.1029/2018GL080280

Bashir, M. F., & Ilie, R. (2021). The first observation of N^+ electromagnetic ion cyclotron waves. *Journal of Geophysical Research: Space Physics*, *126*(3), e2020JA028716. https://doi.org/10.1029/2020JA028716

Berchem, J., Fuselier, S. A., Petrinec, S., Frey, H. U., & Burch, J. L. (2003). Dayside proton aurora: Comparisons between global MHD simulations and IMAGE observations. *Space Science Reviews*, *109*(1), 313–349. https://doi.org/10.1023/B:SPAC.0000007523.23002.92

Blum, L. W., Agapitov, O., Bonnell, J. W., Kletzing, C., & Wygant, J. (2016). EMIC wave spatial and coherence scales as determined from multipoint Van Allen Probe measurements. *Geophysical Research Letters*, *43*(10), 4799–4807. https://doi.org/10.1002/2016GL068799

Blum, L. W., Bonnell, J. W., Agapitov, O., Paulson, K., & Kletzing, C. (2017). EMIC wave scale size in the inner magnetosphere: Observations from the dual Van Allen Probes. *Geophysical Research Letters*, *44*(3), 1227–1233. https://doi.org/10.1002/2016GL072316

Blum, L. W., Halford, A., Millan, R., Bonnell, J. W., Goldstein, J., Usanova, M., et al. (2015). Observations of coincident EMIC wave activity and duskside energetic electron precipitation on 18-19 January 2013. *Geophysical Research Letters*, *42*(14), 5727–5735. https://doi.org/10.1002/2015GL065245

Blum, L. W., Koval, A., Richardson, I. G., Wilson, L. B., Malaspina, D., Greeley, A., & Jaynes, A. N. (2021). Prompt response of the dayside magnetosphere to discrete structures within the sheath region of a coronal mass ejection. *Geophysical Research Letters*, *48*(11), e92700. https://doi.org/10.1029/2021GL092700

Bonnell, J. W., Mozer, F. S., Delory, G. T., Hull, A. J., Ergun, R. E., Cully, C. M., et al. (2008). The electric field instrument (EFI) for THEMIS. *Space Science Reviews*, *141*(1–4), 303–341. https://doi.org/10.1007/s11214-008-9469-2

Burch, J. L., Moore, T. E., Torbert, R. B., & Giles, B. L. (2016). Magnetospheric Multiscale overview and science objectives. *Space Science Reviews*, *199*(1–4), 5–21. https://doi.org/10.1007/s11214-015-0164-9

Capannolo, L., Li, W., Ma, Q., Chen, L., Shen, X. C., Spence, H. E., et al. (2019). Direct observation of subrelativistic electron precipitation potentially driven by EMIC waves. *Geophysical Research Letters*, *46*(22), 12711–12721. https://doi.org/10.1029/2019GL084202

Capannolo, L., Li, W., Ma, Q., Qin, M., Shen, X.-C., Angelopoulos, V., et al. (2023). Electron precipitation observed by ELFIN using proton precipitation as a proxy for electromagnetic ion cyclotron (EMIC) waves. *Geophysical Research Letters*, *50*, e2023GL103519. https://doi.org/10.1029/2023GL103519

Capannolo, L., Li, W., Millan, R., Smith, D., Sivadas, N., Sample, J., & Shekhar, S. (2022). Relativistic electron precipitation near midnight: Drivers, distribution, and properties. *Journal of Geophysical Research (Space Physics)*, *127*(1), e30111. https://doi.org/10.1029/2021JA030111

Chen, H., Gao, X., Lu, Q., & Wang, S. (2019). Analyzing EMIC waves in the inner magnetosphere using long-term Van Allen Probes observations. *Journal of Geophysical Research (Space Physics)*, *124*(9), 7402–7412. https://doi.org/10.1029/2019JA026965

Chen, L., Thorne, R. M., Jordanova, V. K., Wang, C.-P., Gkioulidou, M., Lyons, L., & Horne, R. B. (2010). Global simulation of EMIC wave excitation during the 21 April 2001 storm from coupled RCM-RAM-HOTRAY modeling. *Journal of Geophysical Research (Space Physics)*, *115*(A7), A07209. https://doi.org/10.1029/2009JA015075

Chen, L., Zhu, H., & Zhang, X. (2019). Wavenumber analysis of emic waves. *Geophysical Research Letters*, *46*(11), 5689–5697. https://doi.org/10.1029/2019GL082686

Cooper, M. B., Gerrard, A. J., Lanzerotti, L. J., Soto-Chavez, A. R., Kim, H., Kuzichev, I. V., & Goodwin, L. V. (2021). Mirror instabilities in the inner magnetosphere and their potential for localized ULF wave generation. *Journal of Geophysical Research (Space Physics)*, *126*(2), e28773. https://doi.org/10.1029/2020JA028773

Drozdov, A. Y., Allison, H. J., Shprits, Y. Y., Usanova, M. E., Saikin, A., & Wang, D. (2022). Depletions of multi-MeV electrons and their association to minima in phase space density. *Geophysical Research Letters*, *49*(8), e97620. https://doi.org/10.1029/2021GL097620

Engebretson, M. J., Posch, J. L., Capman, N. S. S., Campuzano, N. G., Bělik, P., Allen, R. C., et al. (2018). MMS, Van Allen probes, GOES 13, and ground-based magnetometer observations of EMIC wave events before, during, and after a modest interplanetary shock. *Journal of Geophysical Research (Space Physics)*, *123*(10), 8331–8357. https://doi.org/10.1029/2018JA025984

Escoubet, C. P., Fehringer, M., & Goldstein, M. (2001). Introduction: The cluster mission. *Annales Geophysicae*, *19*(10/12), 1197–1200. https://doi.org/10.5194/angeo-19-1197-2001

Frey, H. U. (2007). Localized aurora beyond the auroral oval. *Reviews of Geophysics*, *45*(1), RG1003. https://doi.org/10.1029/2005RG000174

Fu, S., Ni, B., Lou, Y., Bortnik, J., Ge, Y., Tao, X., et al. (2018). Resonant scattering of near-equatorially mirroring electrons by Landau resonance with H^+ band EMIC waves. *Geophysical Research Letters*, *45*(20), 10866–10873. https://doi.org/10.1029/2018GL079718

Fuselier, S. A., Gary, S. P., Thomsen, M. F., Claflin, E. S., Hubert, B., Sandel, B. R., & Immel, T. (2004). Generation of transient dayside subauroral proton precipitation. *Journal of Geophysical Research (Space Physics)*, *109*(A12), A12227. https://doi.org/10.1029/2004JA010393

Gamayunov, K. V., & Engebretson, M. J. (2021). Low frequency ULF waves in the Earth's inner magnetosphere: Statistics during coronal mass ejections and seeding of EMIC waves. *Journal of Geophysical Research (Space Physics)*, *126*(8), e29247. https://doi.org/10.1029/2021JA029247

Gamayunov, K. V., & Engebretson, M. J. (2022). Low frequency ULF waves in the Earth's inner magnetosphere: Power spectra during high speed streams and quiet solar wind and seeding of EMIC waves. *Journal of Geophysical Research (Space Physics)*, *127*(11), e2022JA030647. https://doi.org/10.1029/2022JA030647

Gamayunov, K. V., Engebretson, M. J., & Elkington, S. R. (2020). EMIC waves in the Earth's inner magnetosphere as a function of solar wind structures during solar maximum. *Journal of Geophysical Research (Space Physics)*, *125*(9), e27990. https://doi.org/10.1029/2020JA027990

Gamayunov, K. V., & Khazanov, G. V. (2007). Effect of oblique electromagnetic ion cyclotron waves on relativistic electron scattering: Combined Release and Radiation Effects Satellite (CRRES)-based calculation. *Journal of Geophysical Research (Space Physics)*, *112*(A7), A07220. https://doi.org/10.1029/2007JA012300

Halford, A. J., Fraser, B. J., & Morley, S. K. (2015). EMIC waves and plasmaspheric and plume density: CRRES results. *Journal of Geophysical Research (Space Physics)*, *120*(3), 1974–1992. https://doi.org/10.1002/2014JA020338

Hartinger, M., Angelopoulos, V., Moldwin, M. B., Glassmeier, K.-H., & Nishimura, Y. (2011). Global energy transfer during a magnetospheric field line resonance. *Geophysical Research Letters*, *38*(12), L12101. https://doi.org/10.1029/2011GL047846

Hartinger, M. D., Turner, D. L., Plaschke, F., Angelopoulos, V., & Singer, H. (2013). The role of transient ion foreshock phenomena in driving Pc5 ULF wave activity. *Journal of Geophysical Research*, *118*(1), 299–312. https://doi.org/10.1029/2012JA018349

Hartinger, M. D., Welling, D., Viall, N. M., Moldwin, M. B., & Ridley, A. (2014). The effect of magnetopause motion on fast mode resonance. *Journal of Geophysical Research*, *119*(10), 8212–8227. https://doi.org/10.1002/2014JA020401

Hasegawa, A. (1969). Drift mirror instability of the magnetosphere. *Physics of Fluids*, *12*, 2642–2650. https://doi.org/10.1063/1.1692407

Inaba, Y., Shiokawa, K., Oyama, S.-I., Otsuka, Y., Connors, M., Schofield, I., et al. (2021). Multi event analysis of plasma and field variations in source of stable auroral red (SAR) arcs in inner magnetosphere during non storm time substorms. *Journal of Geophysical Research (Space Physics)*, *126*(4), e29081. https://doi.org/10.1029/2020JA029081

Jordanova, V. K., Farrugia, C. J., Thorne, R. M., Khazanov, G. V., Reeves, G. D., & Thomsen, M. F. (2001). Modeling ring current proton precipitation by electromagnetic ion cyclotron waves during the May 14-16, 1997, storm. *Journal of Geophysical Research*, *106*(A1), 7–22. https://doi.org/10.1029/2000JA002008

Jordanova, V. K., Spasojevic, M., & Thomsen, M. F. (2007). Modeling the electromagnetic ion cyclotron wave-induced formation of detached subauroral proton arcs. *Journal of Geophysical Research*, *112*(A8), A08209. https://doi.org/10.1029/2006JA012215

Jun, C.-W., Miyoshi, Y., Kurita, S., Yue, C., Bortnik, J., Lyons, L., et al. (2021). The characteristics of EMIC waves in the magnetosphere based on the van Allen probes and Arase observations. *Journal of Geophysical Research: Space Physics*, *126*(6), e2020JA029001. https://doi.org/10.1029/2020JA029001

Jun, C. W., Yue, C., Bortnik, J., Lyons, L. R., Nishimura, Y., & Kletzing, C. (2019). EMIC wave properties associated with and without injections in the inner magnetosphere. *Journal of Geophysical Research (Space Physics)*, *124*(3), 2029–2045. https://doi.org/10.1029/2018JA026279

Kennel, C. F. (1969). Consequences of a magnetospheric plasma. *Reviews of Geophysics and Space Physics*, *7*(1–2), 379–419. https://doi.org/10.1029/RG007i001p00379

Kennel, C. F., & Petschek, H. E. (1966). Limit on stably trapped particle fluxes. *Journal of Geophysical Research*, *71*, 1–28. https://doi.org/10.1029/jz071i001p00001

Kersten, T., Horne, R. B., Glauert, S. A., Meredith, N. P., Fraser, B. J., & Grew, R. S. (2014). Electron losses from the radiation belts caused by EMIC waves. *Journal of Geophysical Research*, *119*(11), 8820–8837. https://doi.org/10.1002/2014JA020366

Khazanov, G. V., & Gamayunov, K. V. (2007). Effect of electromagnetic ion cyclotron wave normal angle distribution on relativistic electron scattering in outer radiation belt. *Journal of Geophysical Research (Space Physics)*, *112*(A10), A10209. https://doi.org/10.1029/2007JA012282

Khazanov, G. V., Gamayunov, K. V., Gallagher, D. L., Kozyra, J. U., & Liemohn, M. W. (2007). Self-consistent model of magnetospheric ring current and propagating electromagnetic ion cyclotron waves: 2. Wave-Induced ring current precipitation and thermal electron heating. *Journal of Geophysical Research*, *112*(A4), A04209. https://doi.org/10.1029/2006JA012033

Kitamura, N., Kitahara, M., Shoji, M., Miyoshi, Y., Hasegawa, H., Nakamura, S., et al. (2018). Direct measurements of two-way wave-particle energy transfer in a collisionless space plasma. *Science*, *361*(6406), 1000–1003. https://doi.org/10.1126/science.aap8730

Kitamura, N., Shoji, M., Nakamura, S., Kitahara, M., Amano, T., Omura, Y., et al. (2021). Energy transfer between hot protons and electromagnetic ion cyclotron waves in compressional Pc5 ultra low frequency waves. *Journal of Geophysical Research (Space Physics)*, *126*(5), e28912. https://doi.org/10.1029/2020JA028912

Lee, D.-Y., Shin, D.-K., & Choi, C.-R. (2018). Effects of oblique wave normal angle and noncircular polarization of electromagnetic ion cyclotron waves on the pitch angle scattering of relativistic electrons. *Journal of Geophysical Research (Space Physics)*, *123*(6), 4556–4573. https://doi.org/10.1029/2018JA025342

Lee, J. H., & Angelopoulos, V. (2014). Observations and modeling of EMIC wave properties in the presence of multiple ion species as function of magnetic local time. *Journal of Geophysical Research (Space Physics)*, *119*(11), 8942–8970. https://doi.org/10.1002/2014JA020469

Lee, J. H., Turner, D. L., Toledo-Redondo, S., Vines, S. K., Allen, R. C., Fuselier, S. A., et al. (2019). Mms measurements and modeling of peculiar electromagnetic ion cyclotron waves. *Geophysical Research Letters*, *46*(21), 11622–11631. https://doi.org/10.1029/2019GL085182

Lee, J. H., Turner, D. L., Vines, S. K., Allen, R. C., Toledo-Redondo, S., Bingham, S. T., et al. (2021). Application of cold and hot plasma composition measurements to investigate impacts on dusk side electromagnetic ion cyclotron waves. *Journal of Geophysical Research (Space Physics)*, *126*(1), e28650. https://doi.org/10.1029/2020JA028650

Li, Y.-X., Yue, C., Ma, Q., Liu, J., Zong, Q.-G., Zhou, X.-Z., et al. (2022). Simultaneous cross-energy ion response and wave generation after the impact of an interplanetary shock. *Journal of Geophysical Research (Space Physics)*, *127*(11), e2022JA030636. https://doi.org/10.1029/2022JA030636

Liu, N., Jin, Y., He, Z., Yu, J., Li, K., & Cui, J. (2022). Simultaneous evolutions of inner magnetospheric plasmaspheric hiss and EMIC waves under the influence of a heliospheric plasma sheet. *Geophysical Research Letters*, *49*(10), e98798. https://doi.org/10.1029/2022GL098798

Liu, Z. Y., Zong, Q. G., Rankin, R., Zhang, H., Wang, Y. F., Zhou, X. Z., et al. (2022). Simultaneous macroscale and microscale wave-ion interaction in near-earth space plasmas. *Nature Communications*, *13*(1), 5593. https://doi.org/10.1038/s41467-022-33298-6

Liu, S., Xia, Z., Chen, L., Liu, Y., Liao, Z., & Zhu, H. (2019). Magnetospheric Multiscale observation of quasiperiodic EMIC waves associated with enhanced solar wind pressure. *Geophysical Research Letters*, *46*(13), 7096–7104. https://doi.org/10.1029/2019GL083421

Lorentzen, D. A., & Moen, J. (2000). Auroral proton and electron signatures in the dayside aurora. *Journal of Geophysical Research*, *105*(A6), 12733–12746. https://doi.org/10.1029/1999JA900405

Loto'Aniu, T. M., Fraser, B. J., & Waters, C. L. (2009). The modulation of electromagnetic ion cyclotron waves by Pc 5 ULF waves. *Annales Geophysicae*, *27*(1), 121–130. https://doi.org/10.5194/angeo-27-121-2009

Ma, Q., Li, W., Thorne, R. M., Ni, B., Kletzing, C. A., Kurth, W. S., et al. (2015). Modeling inward diffusion and slow decay of energetic electrons in the Earth's outer radiation belt. *Geophysical Research Letters*, *42*(4), 987–995. https://doi.org/10.1002/2014GL062977

Ma, Q., Li, W., Yue, C., Thorne, R. M., Bortnik, J., Kletzing, C. A., et al. (2019). Ion heating by electromagnetic ion cyclotron waves and magnetosonic waves in the Earth's inner magnetosphere. *Geophysical Research Letters*, *46*(12), 6258–6267. https://doi.org/10.1029/2019GL083513

McFadden, J. P., Carlson, C. W., Larson, D., Ludlam, M., Abiad, R., Elliott, B., et al. (2008). The THEMIS ESA plasma instrument and in-flight calibration. *Space Science Reviews*, *141*(1–4), 277–302. https://doi.org/10.1007/s11214-008-9440-2

Millan, R. M., & Thorne, R. M. (2007). Review of radiation belt relativistic electron losses. *Journal of Atmospheric and Solar-Terrestrial Physics*, *69*(3), 362–377. https://doi.org/10.1016/j.jastp.2006.06.019

Min, K., Lee, J., Keika, K., & Li, W. (2012). Global distribution of EMIC waves derived from THEMIS observations. *Journal of Geophysical Research (Space Physics)*, *117*(A5), A05219. https://doi.org/10.1029/2012JA017515

Miyoshi, Y., Matsuda, S., Kurita, S., Nomura, K., Keika, K., Shoji, M., et al. (2019). Emic waves converted from equatorial noise due to m/q = 2 ions in the plasmasphere: Observations from Van Allen probes and Arase. *Geophysical Research Letters*, *46*(11), 5662–5669. https://doi.org/10.1029/2019GL083024

Murphree, J. S., Elphinstone, R. D., Hearn, D., & Cogger, L. L. (1990). Large-scale high-latitude dayside auroral emissions. *Journal of Geophysical Research*, *95*(A3), 2345–2354. https://doi.org/10.1029/JA095iA03p02345

Ni, B., Cao, X., Shprits, Y. Y., Summers, D., Gu, X., Fu, S., & Lou, Y. (2018). Hot plasma effects on the cyclotron-resonant pitch-angle scattering rates of radiation belt electrons due to EMIC waves. *Geophysical Research Letters*, *45*(1), 21–30. https://doi.org/10.1002/2017GL076028

Nishimura, Y., Bortnik, J., Li, W., Thorne, R. M., Ni, B., Lyons, L. R., et al. (2013). Structures of dayside whistler-mode waves deduced from conjugate diffuse aurora. *Journal of Geophysical Research (Space Physics)*, *118*(2), 664–673. https://doi.org/10.1029/2012JA018242

Pedersen, A., Lybekk, B., André, M., Eriksson, A., Masson, A., Mozer, F. S., et al. (2008). Electron density estimations derived from spacecraft potential measurements on Cluster in tenuous plasma regions. *Journal of Geophysical Research (Space Physics)*, *113*(A7), A07S33. https://doi.org/10.1029/2007JA012636

Pedersen, A., Mozer, F., & Gustafsson, G. (1998). Electric field measurements in a tenuous plasma with spherical double probes. In R. F. Pfaff, J. E. Borovsky, & D. T. Young (Eds.), *Measurement techniques in space plasmas*. https://doi.org/10.1002/9781118664391.ch1

Rae, I. J., Mann, I. R., Watt, C. E. J., Kistler, L. M., & Baumjohann, W. (2007). Equator-S observations of drift mirror mode waves in the dawnside magnetosphere. *Journal of Geophysical Research (Space Physics)*, *112*(A11), A11203. https://doi.org/10.1029/2006JA012064

Rème, H., Aoustin, C., Bosqued, J. M., Dandouras, I., Lavraud, B., Sauvaud, J. A., et al. (2001). First multispacecraft ion measurements in and near the Earth's magnetosphere with the identical Cluster ion spectrometry (CIS) experiment. *Annales Geophysicae*, *19*(10/12), 1303–1354. https://doi.org/10.5194/angeo-19-1303-2001

Ross, J. P. J., Glauert, S. A., Horne, R. B., Watt, C. E. J., & Meredith, N. P. (2021). On the variability of EMIC waves and the consequences for the relativistic electron radiation belt population. *Journal of Geophysical Research (Space Physics)*, *126*(12), e29754. https://doi.org/10.1029/2021JA029754

Runov, A., Angelopoulos, V., Gabrielse, C., Liu, J., Turner, D. L., & Zhou, X.-Z. (2015). Average thermodynamic and spectral properties of plasma in and around dipolarizing flux bundles. *Journal of Geophysical Research*, *120*(6), 4369–4383. https://doi.org/10.1002/2015JA021166

Shahid, M., Bashir, M. F., Artemyev, A. V., Zhang, X.-J., Angelopoulos, V., & Murtaza, G. (2024). Electromagnetic ion cyclotron emission from ion-scale magnetic holes. *Physics of Plasmas*, *31*(7), 072103. https://doi.org/10.1063/5.0205942

Shumko, M., Gallardo-Lacourt, B., Halford, A. J., Blum, L. W., Liang, J., Miyoshi, Y., et al. (2022). Proton aurora and relativistic electron microbursts scattered by electromagnetic ion cyclotron waves. *Frontiers in Astronomy and Space Sciences*, *9*, 975123. https://doi.org/10.3389/fspas.2022.975123

Sigernes, F., Fasel, L. G., Minow, J., Deehr, C. S., Smith, R. W., Lorentzen, D. A., et al. (1996). Calculations and ground-based observations of pulsed proton events in the dayside aurora. *Journal of Atmospheric and Terrestrial Physics*, *58*(11), 1281–1291. https://doi.org/10.1016/0021-9169(95)00113-1

Sigsbee, K., Kletzing, C. A., Faden, J., & Smith, C. W. (2023). Occurrence rates of electromagnetic ion cyclotron (emic) waves with rising tones in the Van Allen Probes data set. *Journal of Geophysical Research: Space Physics*, *128*(2), e2022JA030548. https://doi.org/10.1029/2022JA030548

Sonnerup, B. U. Ö., & Scheible, M. (2000). Minimum variance analysis, Chapter 8. In G. Paschmann & W. D. Patrick (Eds.), *ISSI book on analysis methods for multi-spacecraft data* (Vol. 449, p. 185).

Soto-Chavez, A. R., Lanzerotti, L. J., Manweiler, J. W., Gerrard, A., Cohen, R., Xia, Z., et al. (2019). Observational evidence of the drift-mirror plasma instability in Earth's inner magnetosphere. *Physics of Plasmas*, *26*(4), 042110. https://doi.org/10.1063/1.5083629

Stix, T. H. (1962). *The theory of plasma waves*. McGraw-Hill.

Summers, D., Ni, B., & Meredith, N. P. (2007). Timescales for radiation belt electron acceleration and loss due to resonant wave-particle interactions: 2. Evaluation for VLF chorus, ELF hiss, and electromagnetic ion cyclotron waves. *Journal of Geophysical Research*, *112*(A4), 4207. https://doi.org/10.1029/2006JA011993

Summers, D., & Thorne, R. M. (2003). Relativistic electron pitch-angle scattering by electromagnetic ion cyclotron waves during geomagnetic storms. *Journal of Geophysical Research*, *108*(A4), 1143. https://doi.org/10.1029/2002JA009489

Thorne, R. M., Horne, R. B., Jordanova, V. K., Bortnik, J., & Glauert, S. (2006). Interaction of EMIC waves with thermal plasma and radiation belt particles. In K. Takahashi, P. J. Chi, R. E. Denton, & R. L. Lysak (Eds.), *Magnetospheric ULF waves: Synthesis and new directions* (Vol. 169, pp. 213–223). https://doi.org/10.1029/169GM14

Turner, D. L., Angelopoulos, V., Shprits, Y., Kellerman, A., Cruce, P., & Larson, D. (2012). Radial distributions of equatorial phase space density for outer radiation belt electrons. *Geophysical Research Letters*, *39*(9), L09101. https://doi.org/10.1029/2012GL051722

Usanova, M. E. (2021). Energy exchange between electromagnetic ion cyclotron (EMIC) waves and thermal plasma: From theory to observations. *Frontiers in Astronomy and Space Sciences*, *8*, 150. https://doi.org/10.3389/fspas.2021.744344

Usanova, M. E., Darrouzet, F., Mann, I. R., & Bortnik, J. (2013). Statistical analysis of EMIC waves in plasmaspheric plumes from Cluster observations. *Journal of Geophysical Research (Space Physics)*, *118*(8), 4946–4951. https://doi.org/10.1002/jgra.50464

Usanova, M. E., Drozdov, A., Orlova, K., Mann, I. R., Shprits, Y., Robertson, M. T., et al. (2014). Effect of EMIC waves on relativistic and ultrarelativistic electron populations: Ground-based and Van Allen Probes observations. *Geophysical Research Letters*, *41*(5), 1375–1381. https://doi.org/10.1002/2013GL059024

Usanova, M. E., Mann, I. R., Bortnik, J., Shao, L., & Angelopoulos, V. (2012). THEMIS observations of electromagnetic ion cyclotron wave occurrence: Dependence on AE, SYMH, and solar wind dynamic pressure. *Journal of Geophysical Research*, *117*(A10), 10218. https://doi.org/10.1029/2012JA018049

Wang, B., Li, P., Huang, J., & Zhang, B. (2019). Nonlinear Landau resonance between EMIC waves and cold electrons in the inner magnetosphere. *Physics of Plasmas*, *26*(4), 042903. https://doi.org/10.1063/1.5088374

Wang, B., Nishimura, Y., Hietala, H., Lyons, L., Angelopoulos, V., Plaschke, F., et al. (2018). Impacts of magnetosheath high-speed jets on the magnetosphere and ionosphere measured by optical imaging and satellite observations. *Journal of Geophysical Research*, *123*(6), 4879–4894. https://doi.org/10.1029/2017JA024954

Wang, B., Nishimura, Y., Zhang, H., Shen, X.-C., Lyons, L., Angelopoulos, V., et al. (2019b). The 2-D structure of foreshock-driven field line resonances observed by THEMIS satellite and ground-based imager conjunctions. *Journal of Geophysical Research (Space Physics)*, *124*(8), 6792–6811. https://doi.org/10.1029/2019JA026668

Xue, Z., Yuan, Z., Yu, X., Deng, D., Huang, Z., & Raita, T. (2022). EMIC waves observed throughout the inner magnetosphere driven by abrupt enhancement of the solar wind pressure. *Geophysical Research Letters*, *49*(9), e98954. https://doi.org/10.1029/2022GL098954

Xue, Z., Yuan, Z., Yu, X., Huang, Z., & Deng, D. (2023). Enhanced solar wind dynamic pressure as a driver of low-energy proton temperature anisotropies and high-frequency emic waves. *Journal of Geophysical Research: Space Physics*, *128*(9), e2023JA031929. https://doi.org/10.1029/2023ja031929

Yahnin, A. G., Yahnina, T. A., Raita, T., & Manninen, J. (2017). Ground pulsation magnetometer observations conjugated with relativistic electron precipitation. *Journal of Geophysical Research (Space Physics)*, *122*(9), 9169–9182. https://doi.org/10.1002/2017JA024249

Yahnin, A. G., Yahnina, T. A., Semenova, N. V., Gvozdevsky, B. B., & Pashin, A. B. (2016). Relativistic electron precipitation as seen by NOAA POES. *Journal of Geophysical Research (Space Physics)*, *121*(9), 8286–8299. https://doi.org/10.1002/2016JA022765

Yan, Y., Yue, C., Ma, Q., Zhou, X.-Z., Zong, Q.-G., Fu, H., et al. (2023). Prompt appearance of large-amplitude emic waves induced by solar wind dynamic pressure enhancement and the subsequent relativistic electron precipitation. *Journal of Geophysical Research: Space Physics*, *128*(7), e2023JA031399. https://doi.org/10.1029/2023JA031399

Yin, Z.-F., Zhou, X.-Z., Hu, Z.-J., Yue, C., Zong, Q.-G., Hao, Y.-X., et al. (2022). Localized excitation of electromagnetic ion cyclotron waves from anisotropic protons filtered by magnetic dips. *Journal of Geophysical Research (Space Physics)*, *127*(6), e30531. https://doi.org/10.1029/2022JA030531

Young, D. T., Burch, J. L., Gomez, R. G., De Los Santos, A., Miller, G. P., Wilson, P., et al. (2016). Hot plasma composition analyzer for the magnetospheric Multiscale mission. *Space Science Reviews*, *199*(1–4), 407–470. https://doi.org/10.1007/s11214-014-0119-6

Yu, X., Yuan, Z., & Ouyang, Z. (2021). First observations of o2+ band emic waves in the terrestrial magnetosphere. *Geophysical Research Letters*, *48*(19), e2021GL094681. https://doi.org/10.1029/2021GL094681

Yuan, Z., Yu, X., Wang, D., Huang, S., Li, H., Yu, T., et al. (2016). In situ evidence of the modification of the parallel propagation of emic waves by heated he+ ions. *Journal of Geophysical Research: Space Physics*, *121*(7), 6711–6717. https://doi.org/10.1002/2016ja022573

Zhang, X.-J., Li, W., Thorne, R. M., Angelopoulos, V., Bortnik, J., Kletzing, C. A., et al. (2016). Statistical distribution of EMIC wave spectra: Observations from van allen probes. *Geophysical Research Letters*, *43*(24), 12. https://doi.org/10.1002/2016GL071158